Monthly Notices of the ROYAL ASTRONOMICAL SOCIETY

MNRAS **499,** 4526–4533 (2020) doi:10.1093/mnras/staa3145
Advance Access publication 2020 October 12

What if the neutron star maximum mass is beyond ∼2.3 $M_\odot$?

X. H. Wu ,★ S. Du and R. X. Xu★
School of Physics, Peking University, Beijing 100871, China

Accepted 2020 October 9. Received 2020 October 9; in original form 2020 July 30

ABSTRACT

By assuming the formation of a black hole soon after the merger event of GW170817, the maximum mass of non-rotating stable neutron star, $M_{\rm TOV} \simeq 2.3\,{\rm M}_\odot$, is proposed by numerical relativity, but there is no solid evidence to rule out $M_{\rm TOV} > 2.3\,{\rm M}_\odot$ from the point of both microphysical and astrophysical views. It is naturally expected that the equation of state (EOS) would become stiffer beyond a specific density to explain massive pulsars. We consider the possibility of EOSs with $M_{\rm TOV} > 2.3\,{\rm M}_\odot$, investigating the stiffness and the transition density in a polytropic model, for two kinds of neutron stars (i.e. gravity-bound and strong-bound stars on surface). Only two parameters are input in both cases: ($\rho_{\rm t}$, γ) for gravity-bound neutron stars, while ($\rho_{\rm s}$, γ) for strong-bound strange stars, with $\rho_{\rm t}$ the transition density, $\rho_{\rm s}$ the surface density, and γ the polytropic exponent. In the matter of $M_{\rm TOV} > 2.3\,{\rm M}_\odot$ for the maximum mass and $70 \leq \Lambda_{1.4} \leq 580$ for the tidal deformability, it is found that the smallest $\rho_{\rm t}$ and γ should be ∼0.50 ρ_0 and ∼2.65 for neutron stars, respectively, whereas for strange star, we have $\gamma > 1.40$ if $\rho_{\rm s} > 1.0\ \rho_0$ (ρ_0 is the nuclear saturation density). These parametric results could guide further research of the real EOS with any foundation of microphysics if a pulsar mass higher than $2.3\,{\rm M}_\odot$ is measured in the future, especially for an essential comparison of allowed parameter space between gravity-bound and strong-bound compact stars.

Key words: equation of state – stars: neutron – pulsars: general.

1 INTRODUCTION

Neutron stars are the densest objects known in the Universe, typically with a mass ∼1.4 $M_\odot$ and a radius ∼10 km. The equation of state (EOS) of neutron star matter is a key issue in relativistic astrophysics and nuclear physics (Weber 2005), that the properties of ultra dense nuclear matter and its associated EoSs are related to bulk stellar properties (mass, radius, moment of inertia), thermal evolution, supernova, gamma-ray bursts, soft gamma repeaters, low-mass X-ray binary, ground state of strong interaction, colour-superconductivity, and other neutron star or nuclear physics phenomena. Currently, the sign problem prevents us from predicting the properties of cold dense matter in the first-principle calculations such as the lattice QCD Monte Carlo simulations, so that phenomenological approaches are developed to explore the inner part of neutron stars.

Nuclear physicists developed many-body theories to describe the neutron star matter (dense matter) EOS, which is unclear at high density, such as Green Function Monto Carlo method (Pieper & Wiringa 2001), chiral perturbation theory (Gasser & Leutwyler 1984, 1985), Brueckner–Hartree–Fock (Brockmann & Machleidt 1971), quark mean field (QMF) model (Toki et al. 1998), quark meson coupling model (Guichon 1988, Saito & Thomas 1994), relativistic mean field (RMF) model (Serot & Walecka 1986), and Nambu–Jona–Lasinio model (Nambu & Jona-Lasinio 1961). Conventionally, a normal neutron star could divided into the core and the crust parts. The outer crust below the neutron drip density, which is composed by nuclei arranged in lattices and relativistic electron gas, provides a negligible contribution to the maximum mass, $M_{\rm TOV}$ (Pearson, Goriely & Chamel 2011). The EOSs of this part are mainly determined by finite-nuclei mass that have slight differences (we show a set of comparison in Fig. 1 below). The Baym–Pethick–Sutherland (BPS; Baym, Pethick & Sutherland 1971) EOS is commonly used to describe the neutron star out crust. The core and inner crust are demarcated by the crust–core transition, where nuclei split into uniform nucleus matter. Nucleus together with leptons forms the core under the β equilibrium. However, a neutron star could actually be a so-called strange quark star if Witten's conjecture is correct (Witten 1984, Alcock, Farhi & Olinto 1986, Haensel, Zdunik & Schaefer 1986), with free quarks to be the composition. Furthermore, a strange star could be in a solid state if quarks are condensed in position space (Xu 2003), and the basic unit of such a star is strangeon (formally called strange quark cluster; Lai & Xu 2017).

We may generally classify the neutron star models into two categories, i.e. gravity-bound stars and strong-bound ones. Due to the large asymmetry of neutron and proton (essentially the asymmetry of up and down quarks), a high number density of electrons would be necessary to suppress the β-decay of neutron to proton. Normal matter bound by gravity on surface could meet the standard of such an electron density, and the conventional neutron stars are therefore gravity-bound, which usually have smaller radii with larger masses. In an analogy to stable atomic nuclei with two-flavour symmetry, three-flavoured strange matter is also supposed to be absolutely stable on surface, i.e. self-confined by strong force. Stellar radius becomes larger as the mass increases for such strong-bound strange

★ E-mail: x.h.wu@pku.edu.cn (XHW); r.x.xu@pku.edu.cn (RXX)

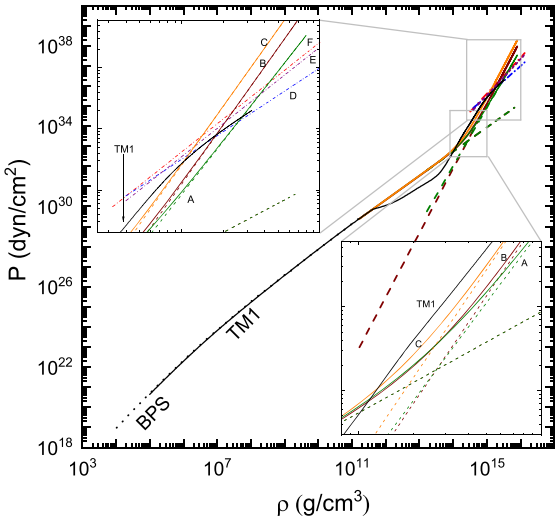

Figure 1. The EOS for gravity-bound and strong-bound star. The solid lines A (ρ_t/ρ_0, γ) = (1.0, 2.9), B (ρ_t/ρ_0, γ) = (1.0, 3.2) and C (ρ_t/ρ_0, γ) = (0.7, 3.2) are neutron star EOS; the dash–dotted lines D (ρ_s/ρ_0, γ) = (1.5, 1.5), E (ρ_s/ρ_0, γ) = (1.5, 1.8), and F (ρ_s/ρ_0, γ) = (1.2, 1.8) are strong-bound star EOS. The dashed lines indicate the corresponding two origin pressure–density relations for EOS A, B, and C. The thin solid line is the TM1 EOS. The dotted line is the BPS EOS.

stars (either strange quark star or strangeon star). The EOS difference of the gravity-bound and strong-bound stars is an interesting issue, and we will measure this latter.

Bulk neutron star observation properties give constraints on the EOS, among which maximum mass ($M_{\rm TOV}$), tidal deformability (Λ), and moment of inertia (I) are dynamical and model-independent measurements. We involve only the maximum mass and the tidal deformability constraints in our calculation, since the measurement of moment of inertia has insufficient precision at present. The 2 $M_\odot$ pulsar observations [PSR J0348+0432 (Antoniadis et al. 2013), PSR J1614-2230 (Demorest et al. 2010, Fonseca et al. 2016), MSP J0740+6620 (Cromartie et al. 2020)] have imposed a lower strict bound to the maximum mass of neutron stars. Therefore a very stiff EOS is required to fulfill this mass constraint. Recently, the neutron star merger event GW170817 offers a new probe to EOS of dense matter, which provides a limit of 1.4 $M_\odot$ tidal deformability, $70 \leq \Lambda_{1.4} \leq 580$ with low-spin (Abbott et al. 2017, 2018b). High-spin $\Lambda_{1.4}$ or binary tidal deformability $\tilde{\Lambda}$ may give different results (Abbott et al. 2017, 2018a, De et al. 2018). Since the low-spin result is in agreement with expectations from binary neutron star spin measurements, we will use this constraint in our paper. From various many-body methods and the tidal deformability up limit, a roughly consistent 1.4 $M_\odot$ neutron star radius constraint refers $R_{1.4} \leq 13.6$ km (Annala et al. 2018; Tews; Margueron & Reddy 2018; Krastev & Li 2019), using the original findings $\Lambda_{1.4} \leq 800$ (Abbott et al. 2017). Based on NASA's Neutron Star Interior Composition Explorer (NICER; Gendreau et al. 2016) data set, it is able to estimate neutron star mass and radii using X-ray pulse-profile modelling (Raaijmakers et al. 2019). Neutron star radii as an observable quantity is valuable to restrict the EOS. So, we conclude this $R_{1.4} \leq 13.6$ km bound in our paper as a contrast of the $\Lambda_{1.4}$ constraint. The stiffness of EOS plays the key role to determine neutron star maximum mass, i.e. stiffer EOSs are required for massive neutron stars. On the other hand, small radii detection results (Raaijmakers et al. 2019) and constraints (Capano et al. 2020), at least for some objects, seems implying soft EOS in low-density range. We focus on the EOS stiffness and its density range in this paper.

It is believed the merger event GW170817 may form a transitory state like hypermassive or supermassive neutron star and eventually becomes black hole. Based on this assumption, upper bounds on $M_{\rm TOV}$ supported by the EOS are placed to be $M_{\rm TOV} \lesssim 2.3\,M_\odot$. By combining the total binary mass of GW170817 and electromagnetic signal, Margalit & Metzger (2017) places an upper limit of $M_{\rm TOV} \lesssim 2.17\,M_\odot$. The boundary $M_{\rm TOV} \lesssim 2.28\,M_\odot$ is derived to limit the ratio of the uniformly rotating neutron star maximum mass over $M_{\rm TOV}$ (Ruiz, Shapiro & Tsokaros 2018). From basic quasiuniversal relations between $M_{\rm TOV}$ and rotating maximum mass, a similar upper limit is set to be $M_{\rm TOV} \lesssim 2.33\,M_\odot$ (Rezzolla, Most & Weih 2018). Shibata et al. (2019) employing the energy and angular momentum conservation laws and numerical-relativity simulations get the cold spherical neutron star EOSs, which gives maximum mass $M_{\rm TOV} \lesssim 2.3\,M_\odot$. $M_{\rm TOV} \lesssim 2.32\,M_\odot$ is obtained from the 15–23 per cent assumption of the relation between maximum baryonic mass and maximum gravitational mass (Abbott et al. 2020a). A measured mass of PSR J2215+5135 from millisecond pulsars gives $2.27^{+0.17}_{-0.15}M_\odot$ (Linares, Shahbaz & Casares 2018). However the $M_{\rm TOV} \lesssim 2.3\,M_\odot$ constraint may be exceeded if the final remain is a stable supermassive neutron star rather than a black hole. A strange star could have $M_{\rm TOV} \sim 2.32\ M_\odot$ when considering colour-flavour locking phase (Zhou, Zhou & Li 2018). A 2.50–2.67 $M_\odot$ compact object is detected in the binary merger event GW190814 (Abbott et al. 2020b), which could either be the heaviest known neutron star or the lightest known black hole. The maximum mass constraint should be beyond 2.3 $M_\odot$ if this 2.6 $M_\odot$ compact object is a neutron star. Godzieba et al. (2020) use a Markov Chain Monte Carlo approach to generate phenomenological EOSs and find that the presence of a normal neutron star in GW190814 is consistent with present astronomical constraints. Parameter set BigApple (Fattoyev et al. 2020) could generate a 2.6 $M_\odot$ normal neutron star and reproduce the observables of finite nuclei and NICER. $M_{\rm TOV} \geq 2.5\,M_\odot$ could be produced if the degrees of freedom drastic changes (Tan et al. 2020). Due to this black hole remnant assumption of GW170817, we consider this $M_{\rm TOV} \sim 2.3\,M_\odot$ as a supermassive index to consider the possibility of a more massive neutron star.

In view of the difficulty from the first-principle calculation, generally, EOSs have several parameters, but a single two-parameter family could offer an accessible approximation (Ofengeim 2020). Polytropic model (Chandrasekhar 1939; Read et al. 2009; Raithel; Özel & Psaltis 2016) has only two parameters (the polytropic constant, K and the polytropic exponent γ) and could model normal phase or exotic phase (Lai & Xu 2009). Baron, Cooperstein & Kahana (1985) have ever use a polytropic model which use incompressibility as the pressure coefficient, together with the compressible liquid-drop model EOS (Cooperstein 1985). They obtained relative small maximum mass due to small K-parameter.

In this paper, we aim to use the simple two-parameter polytropic model to clarify how stiff the pulsar EOS should be and where the stiff EOS starts under the maximum mass ($M_{\rm TOV} \simeq 2.3\,M_\odot$, $M_{\rm TOV} \geq 2\,M_\odot$), low-spin tidal deformability ($70 \leq \Lambda_{1.4} \leq 580$) and radius ($R_{1.4} \leq 13.6$ km) constraints. Furthermore, we also want to know the essential differences between available two-parameter range of gravity-bound and strong-bound stars. For the gravity-bound neutron star, we apply the BPS EOS on the outer crust, and a two segments polytropic model EOS on the inner crust and core part, while the two segments boundary is insistent with the crust–core boundary but consistent with EOS stiffness transform. Although

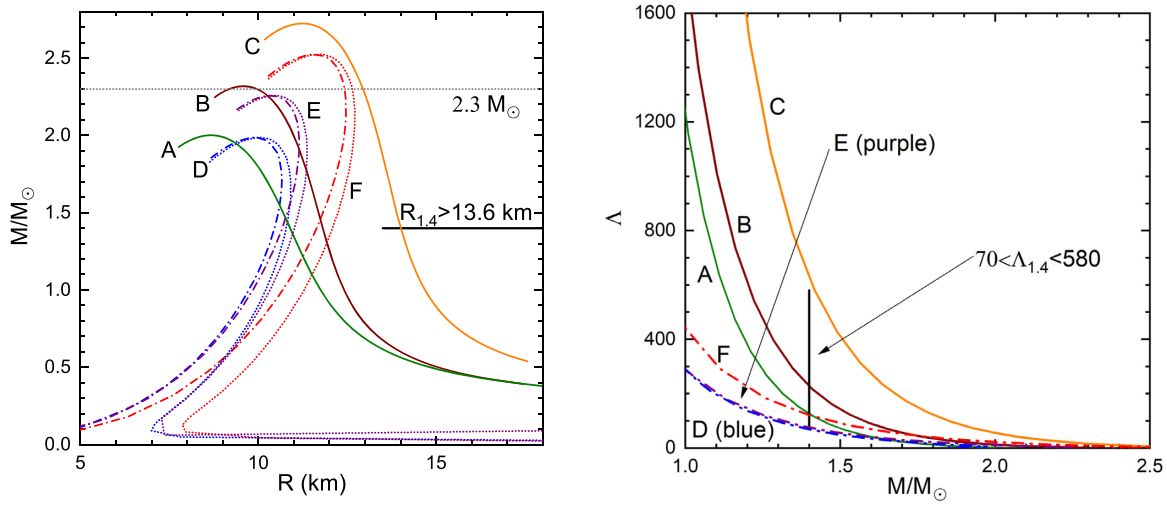

Figure 2. The mass–radius relation (left) and mass-tidal deformabilities relation (right) for gravity-bound and strong-bound stars. The solid lines A (ρ_t/ρ_0, γ) = (1.0, 2.9), B (ρ_t/ρ_0, γ) = (1.0, 3.2), and C (ρ_t/ρ_0, γ) = (0.7, 3.2) are neutron star results; the dash–dotted lines D (ρ_s/ρ_0, γ) = (1.5, 1.5), E (ρ_s/ρ_0, γ) = (1.5, 1.8), and F (ρ_s/ρ_0, γ) = (1.2, 1.8) are strong-bound star results. The dotted lines are strong-bound star with a crust.

two piecewise segments is simple constructed to show the stiffness change with density, this measurement could focus on the stiffer EOS that decisively influence the neutron star maximum mass and radius. Since the EOSs should change uniformly, we merge these two EOS segments smoothly into a new curve, which could still characterize the EOS stiffness change without significant effect on the neutron star mass and radius. Through this way, the newly formed EOS could offer a comparison on the phenomenological EOSs with characteristic stiffness and transition density, to be applicable to the strong bound star EOS too. We apply the two-parameter family polytropic model on these gravity-bound (transition density ρ_t, polytropic exponent γ) and strong-bound (surface density ρ_s, polytropic exponent γ) scenarios, and focus on the mass–radius relation which offers strong constraints. We also compare these two free parameters, measures density range and stiffness, respectively, under the same constraints. The results show that a smaller transition density ρ_t (or surface density ρ_s) and a larger polytrope of exponent γ are always beneficial for stiffer EOS then larger maximum mass. For the neutron star scene, the $R_{1.4}$ constraint limits the transition density which can not be too small. For normal neutron star of $M_{TOV} > 2.3\,M_\odot$, the smallest transition density and polytrope of exponent are (ρ_t/ρ_0, γ) = (0.50, 2.65). While for strange star of $M_{TOV} > 2.3\,M_\odot$, the $\rho_s/\rho_0 = (1.0 \sim 2.0)$ correspond polytropic exponent region should be $\gamma > 1.40$ if $\rho_s/\rho_0 > 1.0$, and also $\rho_s/\rho_0 < 1.58$ when $\gamma < 2.0$. A smaller polytropic exponent in the strong-bound system could derive similar maximum mass than in gravity-bound system. We give details in the results part for reference.

This paper is organized as follows. In the next section, we describe the polytropic model and discuss the selection of these parameters. The gravity-bound and strong-bound scenarios are discussed with two free parameters. In Section 3, we compare the EOS stiffness and mass–radius constraints in the parameter space. There is a conclusion at last.

2 THE MODELS

We apply two kinds of pulsar scenarios, gravity-bound star and strong-bound star. Normal neutron star is a gravity-bound system, which usually has smaller radius with larger mass. In contrast, strange star as the strong-bound system has larger radius with larger mass.

2.1 Gravity-bound object on surface

We assume the neutron star has a soft crust and a hard core to support higher mass. Our EOS is a combination of BPS EOS and a polytropic model. We apply the BPS EOS when $\rho < \rho_{drip}$, with ρ_{drip} the neutron drip out density. We assume a transition density ρ_t, after which the EOS becomes stiff to support a massive core. When $\rho \leq \rho_t$, the pressure is assumed as the extension of the BPS EOS:

$$P_1(\rho) = K_{BPS}\rho^{\gamma_{BPS}}, \tag{1}$$

in which the parameter K_{BPS} and γ_{BPS} are determined by BPS EOS, $P_{BPS}(\rho) = K_{BPS}\rho^{\gamma_{BPS}}$. When $\rho \geq \rho_t$ we have

$$P_2(\rho) = K_2\rho^{\gamma}. \tag{2}$$

At the transition density ρ_t, $P_1(\rho_t) = P_2(\rho_t)$. Then, we have

$$K_2 = K_{BPS}\rho_t^{\gamma_{BPS}}/\rho_t^{\gamma}. \tag{3}$$

We use a new smooth curve to connect the two pressure lines with different exponent γ_{BPS} and γ,

$$P_{ns}(\rho) = A_0\left[\left(\frac{\rho}{\rho_t}\right)^{\gamma_{BPS}\alpha} + \left(\frac{\rho}{\rho_t}\right)^{\gamma\alpha}\right]^{\frac{1}{\alpha}}, \tag{4}$$

where

$$A_0 = K_{BPS}\rho_t^{\gamma_{BPS}}. \tag{5}$$

A larger α means the new curve closer to the origin two lines (the BPS EOS and its extension before ρ_t as well as the stiffer polytropic model EOS). In this paper, α is set as $\alpha = 1$ to obtain a smooth curve. There are two free parameters in this model, the transition density ρ_t and the polytrope of exponent γ.

2.2 Strong-bound object on surface

Strange star (strange quark star and strangeon star) as a strong-bound surface dense matter system has non-zero surface density. We use

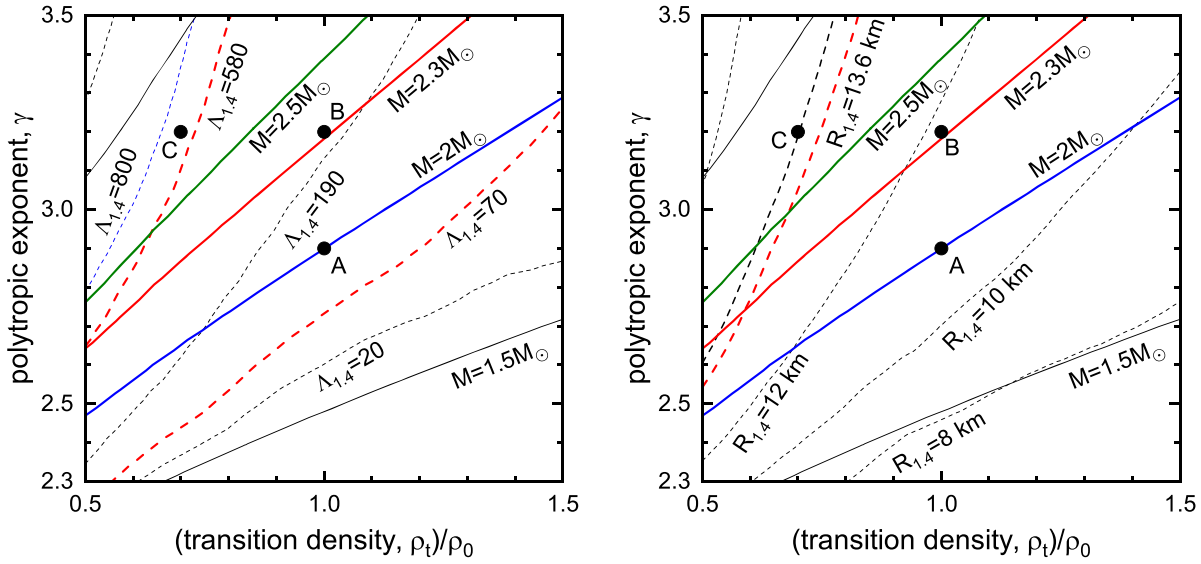

Figure 3. The normal neutron star $M_{\rm TOV}-\Lambda_{1.4}$ (left) and $M_{\rm TOV}-R_{1.4}$ (right) distributions in $\rho_{\rm t}-\gamma$ parameter space. The solid lines show neutron star maximum mass, and the dashed lines represent the 1.4 $M_\odot$ neutron star radius. Points A and B are examples for 2 $M_\odot$ and close to 2.3 $M_\odot$, respectively. Point C is ruled out by $\Lambda_{1.4} \leq 580$ and $R_{1.4} \leq 13.6$ km restricts.

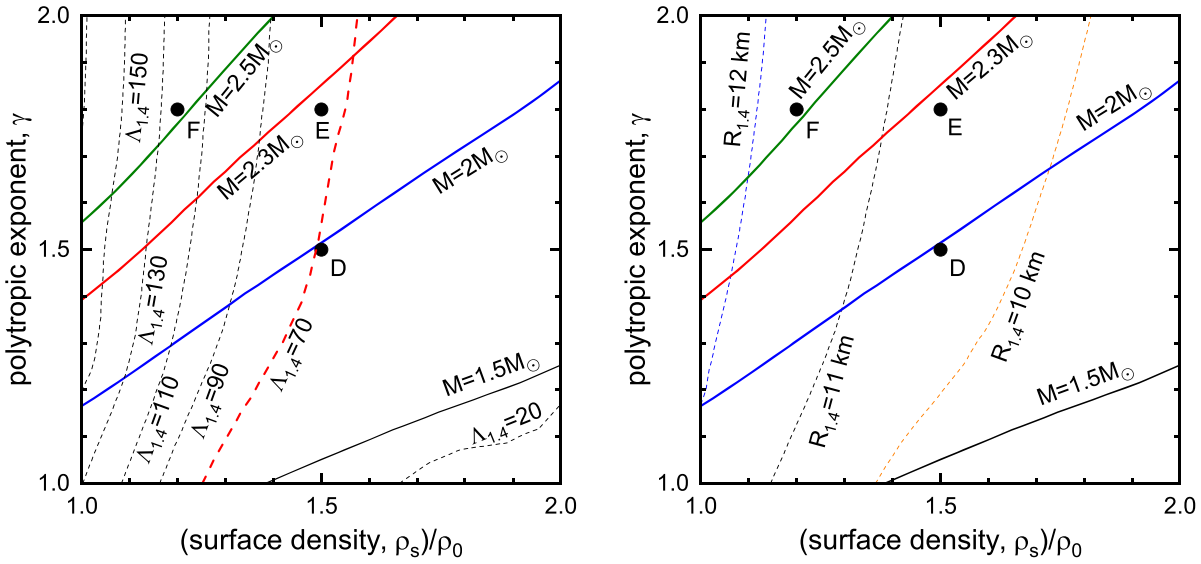

Figure 4. The strange star $M_{\rm TOV}-\Lambda_{1.4}$ (left) and $M_{\rm TOV}-R_{1.4}$ (right) distributions in $\rho_{\rm s}-\gamma$ parameter space. The solid lines indicate strange star maximum mass, and the dashed lines represent the 1.4 $M_\odot$ strange star radius. Points D, E, and F are examples close to 2 $M_\odot$, 2.3 $M_\odot$, and 2.5 $M_\odot$ strong-bound star, respectively. Point D slightly beyond $70 \leq \Lambda_{1.4} \leq 580$ restrict (see also Fig. 2).

the simple polytropic model with the pressure–density form:

$$P_{\rm ss} = K_{\rm ss}\rho^{\gamma}. \tag{6}$$

When $\gamma = 1$, this expression simplified to bag model (Alcock et al. 1986). In this case, with the linear EOS, the bag constant B corresponds to the surface energy, $\rho_{\rm s} = 4B$. strong-bound star has a sharp surface, that the pressure and density will decrease to zero in the *fermi* scale, which will not affect the mass–radius relation. We also involve the possibility that the strange star is enveloped in thin nuclear crusts (e.g. Weber; Kettner & Weigel 1994; Kettner et al. 1995; Huang & Lu 1997; Madsen 1999; Xu 2003; Weber et al. 2012).

The pressure coefficient $K_{\rm ss}$ is determined by the sound speed. Ab initio calculations could constrain the sound speed up to 1 ∼ 2 n_0, but higher densities remain unconstrained (Tews et al. 2018). Polytropic model may result in the superluminal problem due to the sound speed $v_{\rm s} = \sqrt{\partial P/\partial\rho}$ monotonous increase with density, however, Lu et al. (2018) have proved that the actual propagation speed $v_{\rm signal} < c$ is always satisfied without destroying the causality. We assume the stars are relativistic fluid and the sound speed square v_s^2 equals the conformal limit 1/3 at the star surface that is assumed at high density:

$$v_s^2 = \frac{{\rm d}P}{{\rm d}\rho} = K_{\rm ss}\gamma\rho_{\rm s}^{\gamma-1} = \frac{1}{3}. \tag{7}$$

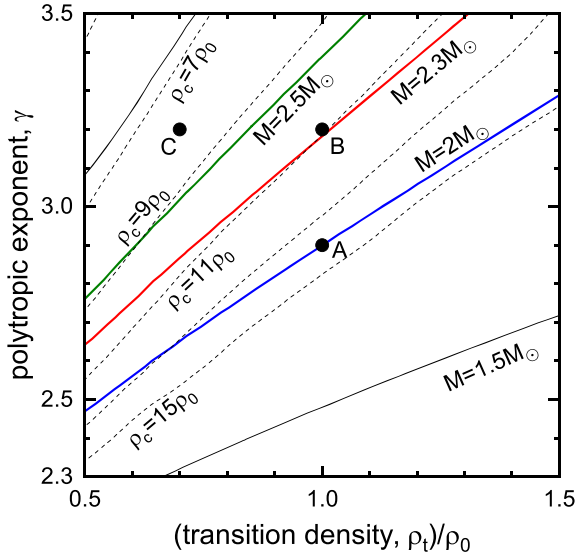

Figure 5. The normal neutron star maximum mass–central density ($M_{\rm TOV}-\rho_0$) distribution in $\rho_{\rm s}-\gamma$ parameter space. The solid lines show neutron star maximum mass, and the dashed lines represent the center density. Points A and B are examples for 2 $M_\odot$ and close to 2.3 $M_\odot$, respectively.

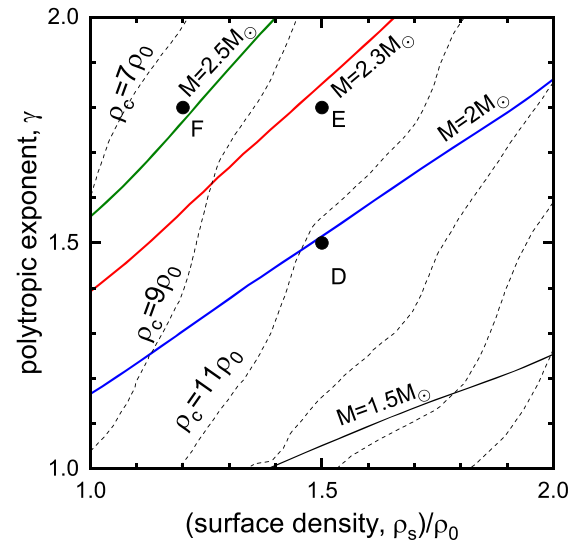

Figure 6. The strong-bound star maximum mass–central density ($M_{\rm TOV}-\rho_0$) distribution in $\rho_{\rm s}-\gamma$ parameter space. The solid lines indicate strange star maximum mass, and the dashed lines represent the center density with 2 ρ_0 spacing. Points D and E are examples close to 2 and 2.3 $M_\odot$ strong-bound star, respectively.

The pressure–density relation becomes

$$P_{\rm ss}(\rho) = \frac{1}{3\gamma\rho_{\rm s}^{\gamma-1}}\rho^{\gamma}, \tag{8}$$

with two free parameters, the surface density $\rho_{\rm s}$, and the polytropic exponent γ.

3 THE RESULTS

The EOS discussed above are shown in Fig. 1. Logarithmic coordinates are used for the abscissa and ordinate, and in that case the curve slope equals the exponent γ with density ρ. We use this nature to extend the BPS EOS to the transition density $\rho_{\rm t}$ for neutron star. The solid lines A ($\rho_{\rm t}/\rho_0$, γ) = (1.0, 2.9), B ($\rho_{\rm t}/\rho_0$, γ) = (1.0, 3.2), and C ($\rho_{\rm t}/\rho_0$, γ) = (0.7, 3.2) connect with BPS EOS are neutron star EOSs, while D ($\rho_{\rm s}/\rho_0$, γ) = (1.5, 1.5), E ($\rho_{\rm s}/\rho_0$, γ) = (1.5, 1.8), and F ($\rho_{\rm s}/\rho_0$, γ) = (1.2, 1.8) are strong-bound star EOSs with a non-zero surface and pressure. Among these EOSs, A (D) and B (E) have the same transition density $\rho_{\rm t}$ (surface density $\rho_{\rm s}$), while B (E) and C (F) have the same polytropic exponent γ. The polytropic exponent γ is the symbol of EOS stiffness. The gravity-bound star EOSs we used has larger polytropic exponent γ compared with the strong-bound star EOSs. The RMF theory with TM1 parameter set provides excellent results for the properties of heavy nuclei ground states and 2.18 $M_\odot$ neutron star (Sugahara & Toki 1994, Shen et al. 2011). We draw the TM1 EOS in Fig. 1 as a comparison. We found that after neutron drip out density there exits a slope decrease, which is considered as one of the reason that TM1 cannot support more massive neutron stars.

Neutron star EOS combines the BPS EOS and a smooth curve derived by two polytropic pressure–density relations with different polytrope of exponent γ, in which the low-density pressure polytropic exponent γ is same as the BPS EOS. Inserting the EOS given by equations (4) and (8) into Tolman–Oppenheimer–Volkoff equation, we have the mass–radius relations for gravity-bound and strong-bound star, see Fig. 2. We also give the tidal deformabilities as a function of neutron star mass in Fig. 2. A smaller transition density also means large radius corresponds to a relatively large mass because the hard core part could extend to lower density. The transition density $\rho_{\rm t} > \rho_0$ gives similar results with other effective models (e.g. HKP020, QMF18, SLy9, DD2, DDME2, NL3-$\omega\rho$; Haensel, Proszynski & Kutschera 1981, Zhu, Zhou & Li 2018). Stiffer EOS gives larger maximum mass and larger tidal deformabilities. But strange star tidal deformabilities are smaller than normal neutron star with similar maximum mass. Line C ($\rho_{\rm t}/\rho_0$, γ) = (0.7, 3.2) exceeds the $\Lambda_{1.4}$ range and breaks the $R_{1.4}$ restrict. Line D has $\Lambda_{1.4} \simeq 68$ that slightly exceeds the $\Lambda_{1.4}$ constraint. Strange quark star or strange on star may have a crust that have a maximum density less than the neutron drip density, so that the Coulomb repulsive force can avoid the crust be absorbed by the strange star. We noticed that the mass–radius relation become normal neutron star like after adding the crust since the crust is gravity-bound by the strange star core. Besides, the crust mass is so small compared to the strong-bound star core that it negligibly increase the star mass but enlarge the radius when the strong-bound star core is not massive enough. Gravity-bound star model A (B) and strong-bound star model D (E) have very similar maximum mass, while neutron star model polytropic exponent γ is larger. This implies a gravity-bound system needs stiffer EOS than strong-bound system to reach the same maximum mass.

Fig. 3 show the maximum mass and 1.4 $M_\odot$ neutron star tidal deformabilities (radius) distributions in the transition density and polytropic exponent ($\rho_{\rm t}-\gamma$) parameter space (which can extend to higher values). Points A and B have the same transition density $\rho_t = 1.0\,\rho_0$, while points B and C have the same polytropic exponent $\gamma = 3.2$. A narrow area starts from ($\rho_{\rm t}/\rho_0$, γ) = (0.50, 2.65) is available for $M \geq 2.3\,M_\odot$ and $\Lambda_{1.4} < 580$. This area can certainly extend to overstep this figure range. The strong constraint $M \geq 2\,M_\odot$ provides wider ($\rho_{\rm t}$, γ) scope. From this figure, a larger polytropic exponent γ is needed to reach neutron star maximum mass limit, and the small transition densities $\rho_{\rm t}$ are restricted by the 1.4 $M_\odot$ tidal deformability. Compared with these two distributions, it is found that radius range 9.8 km $< R_{1.4} <$ 13.8 km roughly consist with $70 \leq \Lambda_{1.4} \leq 580$.

Strange star usually use the surface density $(\rho_s/\rho_0) = (1.0 \sim 2.0)$. Fig. 4 gives the similar distributions for strong-bound object. Points D and E have the same surface density 1.5 ρ_0, while points E and F have the same polytrope of exponent $\gamma = 1.8$. From our calculation, all the parameter range $(\rho_s/\rho_0, \gamma) = (1.0 \sim 2.0, 1.0 \sim 2.0)$ satisfy the $R_{1.4} \leq 13.6$ km limit. But $\Lambda_{1.4} \geq 70$ exclude larger surface density that $\rho_s < 1.58$ if $\gamma < 2.0$. 2 $M_\odot$ strong-bound system needs $\gamma > 1.18$, and $\gamma > 1.40$ for 2.3 $M_\odot$ strong-bound system. strong-bound star scene could have massive maximum mass and relatively small tidal deformability simultaneously. $R_{1.4} < 12.5$ is needed by $\rho_s \geq 1.0$, and $R_{1.4} > 10.5$ is roughly consistent with $\Lambda_{1.4} \geq 70$.

An evidence trend is observed that the pulsar maximum mass increase with larger polytropic exponent γ and smaller transition density ρ_t (surface density ρ_s) for gravity-bound scene (strong-bound scene). An obvious phenomenon is found that the gravity-bound star EOS are stiffer than the strong-bound star to attain similar neutron star maximum mass.

Figs 5 and 6 are the mass and the central density distribution in the $\rho_t(\rho_s) - \gamma$ parameter space for normal neutron star and strange star, respectively. Smaller central density always match with larger maximum mass and normal neutron star has larger central density than strange star with the same maximum mass. The deconfined quark matter is expected to appear at relative high density, beyond where quarks can no longer considered belonging to specific baryons. For a typical baryon radius $r_b = 0.5$ fm, quark percolation could occur at $1/\sqrt{2}(4/3\pi r_b^3)/\rho_0 \approx 8.44\ \rho_0$ (face centre cubic). From which the polytropic exponent should have an alter value that quark matter construction replaced original hadronic matter. In other words, the polytropic model should have another segment. Since the core part contribute most to the neutron star, a smaller transition density (surface density) will lead to smaller central density with the same maximum mass.

4 CONCLUSIONS

The existence of massive neutron star requires stiff core EOS. However, the tidal deformability restrict and supernova explosion prefer a soft normal neutron star crust. We apply the polytropic model to examine how stiff the neutron star EOS should be and the transition density (surface density) range. We apply vanishing surface density for normal neutron star and non-zero surface density for strange star. For the normal neutron star scenario, we merge the two EOS segments smoothly into a new curve, so that the total EOS could change uniformly. To measure and compare normal neutron star and strange star EOSs, we apply the two-parameter family (ρ_t or ρ_s, γ) polytropic model. These two characteristic EOS stiffness and transition density (surface density) parameter space could offer a reasonable range for phenomenological EOS.

A small transition density $\rho_t > 0.50\ \rho_0$ and a large polytropic exponent $\gamma > 2.65$ are beneficial to the $M_{TOV} > 2.3\ M_\odot$ conventional neutron star, while for $M_{TOV} > 2.3\ M_\odot$ strange star, the polytropic exponent $\gamma > 1.40$ is required to $\rho_s \sim 1.0\ \rho_0$. A small transition density ($\rho_t/\rho_0 < 0.50$ for 2.3 $M_\odot$) may break the 1.4 $M_\odot$ tidal deformability restrict, while strong-bound system model requires $\rho_s/\rho_0 < 1.58$ for $\gamma < 2.0$. As a strong-bound system, strange star could have smaller radius and larger mass with the same polytropic exponent compared with normal neutron star. By comparing the $M_{TOV}-\Lambda_{1.4}$ and $M_{TOV}-R_{1.4}$ distributions we derive rough results of common neutron star radius range, which is 9.8 km $< R_{1.4} <$ 13.8 km for normal neutron stars and 10.5 km $< R_{1.4} <$ 12.5 km for strange stars. With this work, we transform the mass–radius and mass-tidal deformability constraints into the stiffness transition density and the polytropic exponent (stiffness measurement parameter) parameter space. These are meaningful for other phenomenological model, especially for an essential comparison of allowed parameter space between gravity-bound and strong-bound compact stars.

ACKNOWLEDGEMENTS

We acknowledge useful discussions at the pulsar group of PKU. This work is supported by the National Key Research and Development of China (Grant Nos. 2018YFA0404703 and 2017YFA0402602), the National Natural Science Foundation of China (Grant Nos. 11673002 and U1531243), and the Strategic Priority Research Program of Chinese Academy of Sciences (Grant No. XDB23010200).

DATA AVAILABILITY

No new data were generated or analysed in support of this research.

REFERENCES

Abbott B. P. et al., 2017, Phys. Rev. Lett., 119, 161101
Abbott B. P. et al., 2018a, Phys. Rev. X, 9, 011001
Abbott B. P. et al., 2018b, Phys. Rev. Lett., 121, 161101
Abbott B. P. et al., 2020a, Class. Quantum Gravity, 37, 45006
Abbott R. et al., 2020b, ApJ, 44, 896
Alcock C., Farhi E., Olinto A., 1986, ApJ, 310, 261
Annala E., Gorda T., Kurkela A., Vuorinen A., 2018, Phys. Rev. Lett., 120, 172703
Antoniadis J. et al., 2013, Science, 340, 448
Baron E., Cooperstein J., Kahana S., 1985, Phys. Rev. Lett., 55, 126
Baym G., Pethick C. J., Sutherland P., 1971, ApJ, 170, 299
Brockmann R., Machleidt R., 1990, Phys. Rev. C, 42, 1965
Capano C. D. et al., 2020, Nat. Astron., 4, 625
Chandrasekhar S., 1939, Introduction to the Study of Stellar Structure. The University of Chicago press, Chicago
Cooperstein J., 1985, Nucl. Phys. A, 438, 722
Cromartie H. T. et al., 2020, Nat. Astron., 4, 72
De S., Finstad D., Lattimer J. M., Brown D. A., Berger E., Biwer C. , 2018, Phys. Rev. Lett., 121, 091102
Demorest P., Pennucci T., Ransom S., Roberts M., Hessels J. W. T., 2010, Nature, 467, 1081
Fattoyev F. J., Horowitz C. J., Piekarewicz J., Reed B., 2020, preprint (arXiv: 2007.03799)
Fonseca E. et al., 2016, ApJ, 832, 167
Gasser J., Leutwyler H., 1984, Ann. Phys., 158, 142
Gasser J., Leutwyler H., 1985, Nucl. Phys. B, 250, 465
Gendreau K. C. et al., 2016, in den Herder J.-W. A., Takahashi T., Bautz M., eds, Proc. SPIE Conf. Ser. Vol. 9905, Space Telescopes and Instrumentation 2016: Ultraviolet to Gamma Ray. SPIE, Bellingham, p. 99051H
Godzieba D. A., Radice D., Bernuzzi S., 2020, preprint (arXiv:2007.10999)
Guichon P. A. M., 1988, Phys. Lett. B, 200, 235
Haensel P., Proszynski M., Kutschera M., 1981, A&A, 102, 299
Haensel P., Zdunik J. L., Schaefer R., 1986, A&A, 160, 121
Huang Y. F., Lu T., 1997, A&A, 325, 189
Kettner Ch., Weber F., Weigel M. K., Glendenning N. K., 1995, Phys. Rev. D, 51, 1440
Krastev P. G., Li B. A., 2019, J. Phys. G, 46, 074001
Kurkela A., Fraga E. S., Schaffner-Bielich J., Vuorinen A., 2014, ApJ, 789, 2
Lai X. Y., Xu R. X., 2009, Astropart. Phys., 31, 128
Lai X. Y., Xu R. X., 2017, J. Phys. Conf. Ser., 861, 012027
Linares M., Shahbaz T., Casares J., 2018, ApJ, 859, 54
Lu J. G., Zhou E. P., Lai X. Y., Xu R. X., 2018, Sci. China-Phys. Mech. Astron., 61, 089511
Madsen J., 1999, in Hadrons in Dense Matter and Hadrosynthesis, Proceedings of the Eleventh Chris Engelbrecht Summer School, 1998. Springer, Berlin, p. 162

Margalit B., Metzger B. D., 2017, ApJ, 850, L19
Nambu Y., Jona-Lasinio G., 1961, Phys. Rev., 122, 345
Ofengeim D. D., 2020, Phys. Rev. D, 101, 103029
Pearson J. M., Goriely S., Chamel N., 2011, Phys. Rev. C, 83, 065810
Pieper S. C., Wiringa R. B., 2001, Annu. Rev. Nucl. Part. Sci., 51, 53
Raaijmakers G. et al., 2019, ApJ, 887, L22
Raithel C. A., Özel F., Psaltis D., 2016, ApJ, 831, 44
Read J. S., Lackey B. D., Owen B. J., Friedman J. L., 2009, Phys. Rev. D, 79, 124032
Rezzolla L., Most E. R., Weih L. R., 2018, ApJ, 852, L25
Ruiz M., Shapiro S. L., Tsokaros A., 2018, Phys. Rev. D, 97, 021501
Saito K., Thomas A. W., 1994, Phys. Lett. B, 327, 9
Serot B. D., Walecka J. D., 1986, Adv. Nucl. Phys., 16, 1
Shen H., Toki H., Oyamatsu K., Sumiyoshi K., 2011, ApJ, 197, 20
Shibata M., Zhou E., Kiuchi K., Fujibayashi S., 2019, Phys. Rev. D, 100, 023015
Sugahara Y., Toki H., 1994, Nucl. Phys. A, 579, 557
Tan H., Noronha-Hostler J., Yunes N., 2020, preprint (arXiv:2006.16296)
Tews I., Margueron J., Reddy S., 2018, Phys. Rev. C, 98, 045804
Tews I., Carlson J., Gandolfi S., Reddy S., 2018, ApJ, 860, 149
Toki H., Meyer U., Faessler A., Brockmann R., 1998, Phys. Rev. C, 58, 3749
Weber F., 2005, Prog. Part. Nucl. Phys., 54, 193
Weber F., Kettner C., Weigel M. K., 1994, Strange-matter Stars, (LBL.36210)
Weber F., Orsaria M., Rodrigues H., Yang S. H., 2012, Proc. Int. Astron. Union, 8, 61
Witten E., 1984, Phys. Rev. D, 30, 272
Xu R. X., 2003, Chin. J. Astron. Astrophys., 3, 33
Zhou E. P., Zhou X., Li A., 2018, Phys. Rev. D, 97, 083015
Zhu Z. Y., Zhou E. P., Li A., 2018, ApJ, 862, 98

APPENDIX A: FURTHER EXPLANATION FOR 2 POLYTROPIC PIECES NORMAL NEUTRON STAR EOS

Typically, three polytropic pieces plus the fixed outer crust are needed to reproduce known EOS models (Read et al.Read et al. 2009, Annala et al. 2018). However, as we have mentioned that the two polytropic pieces with two-parameter family could offer an accessible approximation, and could display the stiffness and transition density intuitively. In this appendix A, we intend to further explain the feasibility of two polytropic pieces through performing the four polytropic pieces EOS and the α parameter effect in equation (4).

Following the work of Kurkela et al.Kurkela et al. (2014), the four polytropic pieces correspond to the outer crust, the inner crust, the nuclear matter, and the perturbative quantum chromodynamics (pQCD) matter, which have polytropic exponent $\gamma_1 = \gamma_{\rm BPS}$, γ_2, γ_3, and $\gamma_4 = 1$ ($v_s^2 = \frac{1}{3}$), respectively. We set the interface densities as $\rho_{\rm drip} = 4 \times 10^{11}\,{\rm g\,cm^{-3}}$ (neutron drip density between outer crust and inner crust), $\rho_{\rm cc} = 0.1\ {\rm fm^{-3}} \approx 1.66 \times 10^{14}\,{\rm g\,cm^{-3}}$ (crust–core interface density, it varies from different model), and $\rho_{\rm pQCD} = (8-10) \times \rho_0$ (pQCD matter, quark percolation, appears). Then, we have the maximum mass and $1.4\,{\rm M}_\odot$ neutron star tidal deformabilities (radius) distributions in the γ_2–γ_3 parameter space (Figs A1 and A2).

Figs A1 and A2 show that to satisfy the $70 \leq \Lambda_{1.4} \leq 580$ constraint, inner crust stiffness γ_2 lies in a range close to $\gamma_{\rm BPS} \approx 1.20$. Therefore, equation (1) is a reasonable assumption, which could consider as the description of outer crust and inner crust (the soft part). Fig. A3 gives the effect of parameter α in equation (4) with the example EOS B (1,3.2). When $\alpha \leq 0.3$, the interpolation pressure keeps away from the origin pressures. When $\alpha \geq 3$, the interpolation pressure keeps very close to the origin pressures and have little effect on the mass–radius relation. $\alpha = 0.5$ gives proper interpolation pressure but larger biased mass–radius relation. We select $\alpha = 1$ in our paper to offer a smooth curve and may present a possible different stiffness between the soft part and the stiff part.

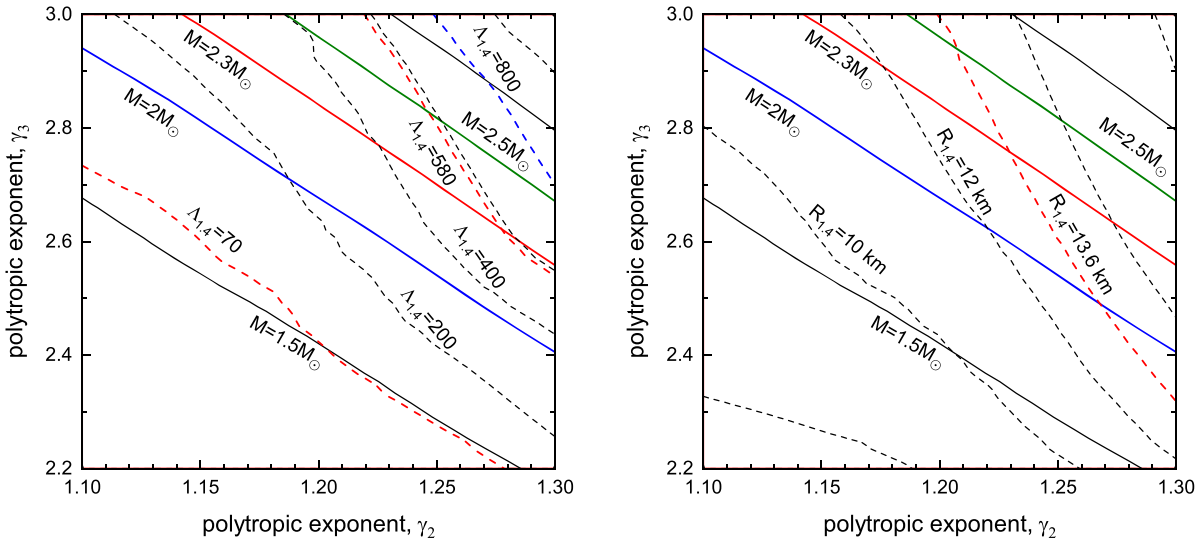

Figure A1. The normal neutron star $M_{\rm TOV}-\Lambda_{1.4}$ (left) and $M_{\rm TOV}-R_{1.4}$ (right) distributions in γ_2–γ_3 parameter space. The solid lines show neutron star maximum mass, and the dashed lines represent the $1.4\,{\rm M}_\odot$ neutron star tidal deformabilities (radius). The pQCD matter appears at $8\rho_0$.

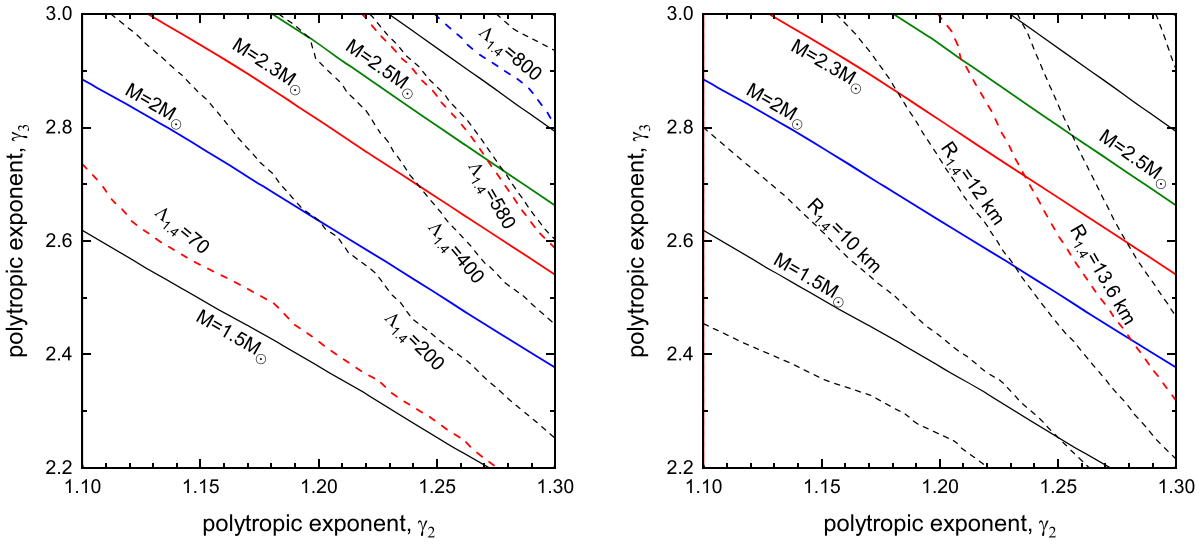

Figure A2. The normal neutron star $M_{\rm TOV}-\Lambda_{1.4}$ (left) and $M_{\rm TOV}-R_{1.4}$ (right) distributions in $\gamma_2-\gamma_3$ parameter space. The solid lines show neutron star maximum mass, and the dashed lines represent the 1.4 $M_\odot$ neutron star tidal deformabilities (radius). The pQCD matter appears at $10\rho_0$.

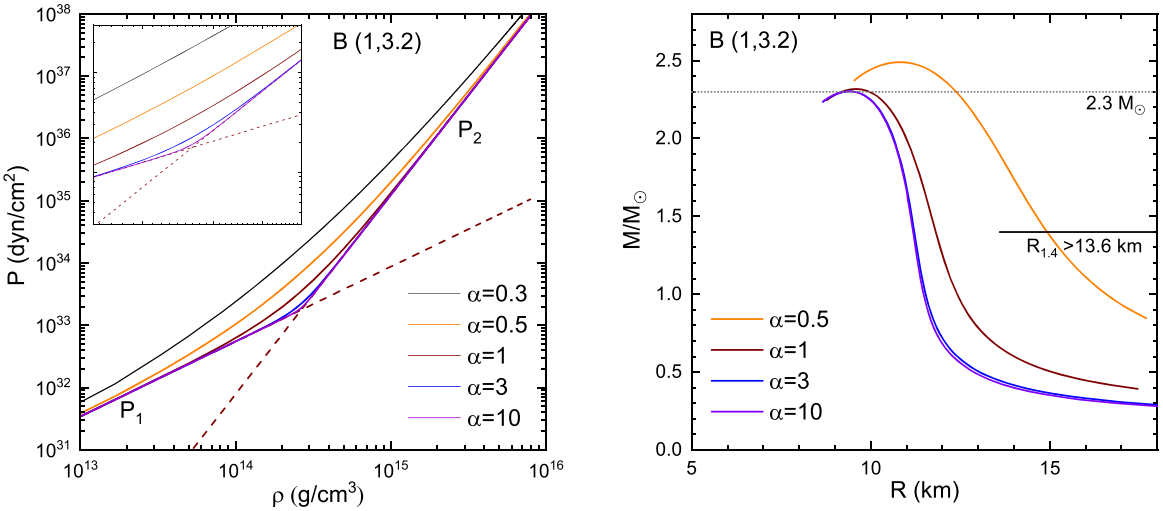

Figure A3. α parameter effect in equation (4).

This paper has been typeset from a TEX/LATEX file prepared by the author.